

Raman Modes of Index-Identified Freestanding Single-Walled Carbon Nanotubes

Jannik C. Meyer,^{1,*} Matthieu Paillet,^{2,†} Thierry Michel,² Alain Moréac,³ Anita Neumann,⁴ Georg S. Duesberg,⁴ Siegmund Roth,¹ and Jean-Louis Sauvajol²

¹Max Planck Institute for Solid State Research, Stuttgart, Germany

²Laboratoire des Verres, Colloïdes et Nanomatériaux (UMR CNRS 5587), Université de Montpellier II, France

³Groupe Matière Condensée et Matériaux (UMR CNRS 6626), Université de Rennes I, France

⁴Infineon Technologies Corporate Research, Munich, Germany

(Received 25 June 2005; published 14 November 2005)

Using electron diffraction on freestanding single-walled carbon nanotubes, we have determined the structural indices (n, m) of tubes in the diameter range from 1.4 to 3 nm. On the same freestanding tubes, we have recorded Raman spectra of the tangential modes and the radial breathing mode. For the smaller diameters (1.4–1.7 nm), these measurements confirm previously established radial breathing mode frequency versus diameter relations and would be consistent with the theoretically predicted proportionality to the inverse diameter. However, for extending the relation to larger diameters, either a yet unexplained environmental constant has to be assumed, or the linear relation has to be abandoned.

DOI: 10.1103/PhysRevLett.95.217401

PACS numbers: 78.30.Na, 61.14.Lj, 73.22.-f, 78.67.Ch

Raman spectroscopy is an important technique in the characterization of carbon nanotubes [1,2]. The characteristic features of the Raman spectrum of single-walled carbon nanotubes (SWNTs) depend on the nanotube structure, defined by the indices (n, m) [3]. The so-called radial breathing mode (RBM) is a fingerprint of single-walled nanotubes, and its frequency is related to the nanotube diameter. The relation of the RBM frequency ω_{RBM} to the nanotube diameter d is often given as $\omega_{\text{RBM}} = A/d + B$. This relation agrees well with various calculations and experiments [1–9]; however, the actual values found for A and B vary significantly. The value of B is interpreted as an effect of the environment (substrate, bundle, or detergent) and is expected to be zero for freestanding nanotubes.

Up to now, there existed no independent determination of the nanotube structure and diameter in combination with its Raman spectrum or the RBM frequency on the same individual nanotubes. We present Raman spectroscopy in combination with an independent determination of the nanotube structure by electron diffraction [10–15]. From the RBM frequencies measured on precisely identified nanotube structures, we obtain an RBM vs diameter relationship that does not depend on any modelization of nanotube electronic or mechanical properties.

The experiments are based on a new simple procedure to create arbitrary nanostructures by electron beam lithography in such a way that access by transmission electron microscope (TEM) is possible. The structures, with the SWNTs embedded, are created on the edge of a cleaved substrate and made freestanding with an etching process [16,17].

SWNTs are grown by chemical vapor deposition on highly doped silicon substrates with a 200 nm silicon dioxide layer [18]. A metal structure consisting of 3 nm Cr and 110 nm Au is created by electron beam lithography on top of the as-grown carbon nanotubes. The substrate is

then cleaved through the metal grid structure. An etching process, as illustrated in Fig. 1, is used to obtain freestanding nanotubes: The sample is etched in a 30% KOH bath at 60 °C for 7 hours. This removes quickly the bulk Si substrate and, slowly, the oxide layer. The etch rate of the doped silicon substrate can be controlled by biasing it with respect to the bath. Since the oxide layer initially acts as a mask, the structure is undercut mainly from the side of the cleaved edge. An undercut of 10 μm can be achieved, and the etching process has to be stopped just when the oxide layer is completely removed. After the etching process, the sample is transferred into deionized water, isopropanol, and acetone before a critical point drying step. On half of

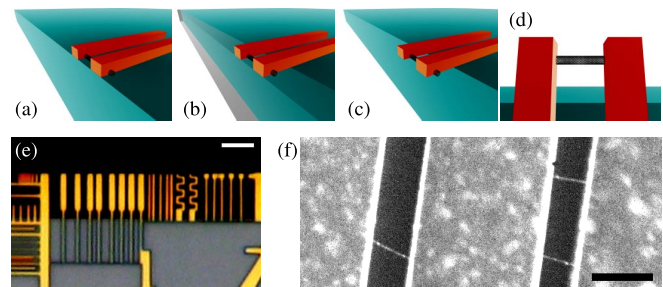


FIG. 1 (color online). Sample preparation procedure: (a) The substrate is cleaved through a metallic grid which is on top of the SWNTs. (b) The sample is etched so that the structure is undercut mainly from the side, removing the shaded volume. The resulting structure (c) reaches out across the side edge of the substrate. Since the nanotube is still held by the metal contacts, and the substrate is no longer in the way, it is accessible for TEM investigations (d), viewed from top. (e) An optical microscope image of a freestanding structure (scale bar 5 μm). The location of SWNTs within the structure is known from overview TEM images (f), so that micro-Raman measurements are possible on precisely located nanotubes. (f) A dark-field mode TEM image. Scale bar is 1 μm .

the freestanding nanotube samples, a tiny amount of silver is deposited by thermal evaporation. The amount corresponding to a 1 nm thick layer forms separated silver particles a few nanometers in diameter along the nanotube [19,20]. Two small particles are visible in Fig. 2(d). We find that the silver deposition on the nanotubes can lead to an increase of the Raman intensity.

Since the substrate is no longer in the way, TEM is possible on the freestanding part of the structure on the edge of the substrate. The SWNTs are held in place by the metal structure. Before the micro-Raman experiments, overview TEM images are obtained at low dose and voltage (60 kV) to get the position and orientation of the SWNTs with respect to the metal structure [Fig. 1(f)].

Since the metal structure is visible in the optical microscope and the overview images show the nanotube location and their orientation with respect to the metal grid, it is possible to carry out micro-Raman experiments on a perfectly localized and oriented single tube. A first series of room-temperature Raman spectra was measured using the Ar/Kr laser lines at 488 nm (2.54 eV), 514.5 nm (2.41 eV), and 647.1 nm (1.92 eV) in the backscattering geometry on a triple subtractive Jobin-Yvon T64000 spectrometer equipped with a liquid nitrogen cooled charge coupled device detector. Another series of spectra were collected using a tunable laser (1.57–1.7 eV) with a Dilor XY800 spectrometer. In all the experiments, the instrumental reso-

lution was 2 cm^{-1} . A precise positioning of the tubes under the laser spot ($1 \mu\text{m}$ laser spot) was monitored with a piezoelectric nanopositioner. In our experimental configuration, the incident light polarization is along the SWNT axis (the Z axis), and no analysis of the polarization of the scattered light is done.

After measuring the Raman spectra, diffraction patterns and high-resolution TEM images of the same nanotubes investigated by Raman spectroscopy are obtained. We record diffraction patterns on image plates in a Zeiss 912 Ω microscope operated at 60 kV. The very straight and well-separated nanotubes obtained by our sample preparation method allow a reliable analysis by electron diffraction. The experimentally obtained diffraction pattern is compared with simulated diffraction patterns, and the nanotube indices and the incidence angle of the simulation are adjusted until the simulated pattern matches the experimental one. We verify that only exactly one pair of indices (n, m) matches the experimental pattern, by checking that the simulated patterns for all nearby indices clearly deviate from the experimental one for any incidence angle. Details of our diffraction analysis procedure are given in Ref. [16]. With an electron diffraction pattern that matches only a single pair of indices (n, m), the diameter is precisely known given the length of the carbon-carbon bond. Our diameter values are based on a C-C distance of 1.42 \AA .

We have obtained spectra from 10 perfectly and unambiguously identified nanotubes: (11, 10) (3 times), (15, 6), (16, 7), (12, 12), (17, 9), (15, 14), (27, 4), and (23, 21) (see additional materials [21]). Furthermore, we measured the spectra from two other tubes that could not be fully identified, but of which diameters were quite precisely determined from the equatorial lines of their diffraction patterns, i.e., $1.64 \pm 0.05 \text{ nm}$ and $2.3 \pm 0.05 \text{ nm}$.

Figure 2 shows the Raman spectra (using a 2.41 eV excitation) and the diffraction pattern of a (11, 10) SWNT. The exact determination of the transition energy of a SWNT requires the measurement of the resonance profiles with a broad set of laser lines [4,5]. However, the measurement of a detectable signal for the 2.41 eV incident energy means that the transition energy of the (11, 10) SWNT is close to 2.41 eV. As expected for an individual SWNT, the Raman spectrum is featured by a single narrow RBM located at 169.5 cm^{-1} (FWHM = 7 cm^{-1}). The profile of the (11, 10) tangential modes (TM) bunch, displayed in Fig. 2(b), is well fitted by using two Lorentzian components located at 1593.5 cm^{-1} (FWHM = 6 cm^{-1}) and 1566 cm^{-1} (FWHM = 7 cm^{-1}). In our scattering geometry, the A symmetry modes are expected to contribute predominantly to the Raman signal. The assignment of the two detected peaks on the (11, 10) Raman spectrum as A modes is coherent with *ab initio* calculations [22] and previously reported results [23]. Concerning the accuracy of our procedure of the localization of the tube, it can be pointed out that we found 3 times the same RBM and TM

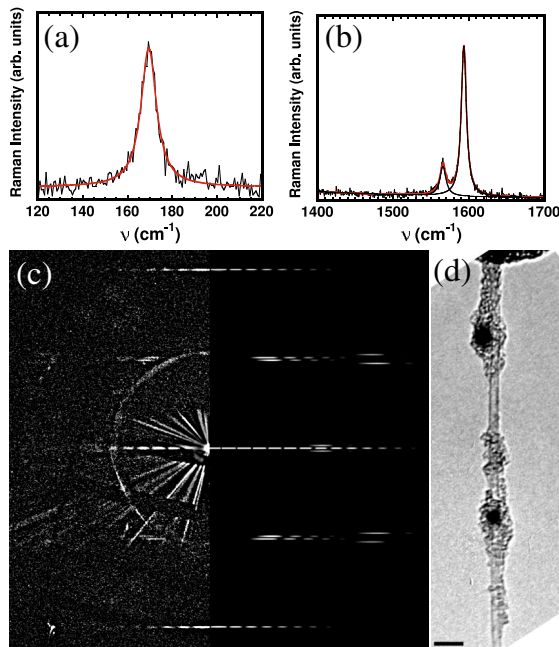


FIG. 2 (color online). (a) RBM and (b) TM ranges of the (11, 10) SWNT ($E_{\text{Laser}} = 2.41 \text{ eV}$). (c) Diffraction pattern of this same (11, 10) nanotube (left: experimental, right: simulated image). (d) High-resolution TEM image of the same nanotube. Two small silver particles are visible, and at the upper end is one of the contacts. Note that most of the amorphous carbon is deposited during the TEM analysis. Scale bar in (d) is 5 nm.

spectra on three different isolated nanotubes identified as (11, 10) from their electron diffraction patterns. The reproduction of the Raman spectra validates our procedure of localization of the tubes. It was recently shown that an uniaxial strain (which could occur on some of our suspended nanotubes) can lead to a downshift of the TM frequencies [24]. From our TM frequencies, we conclude that uniaxial strain (if present) is much smaller in our samples than in Ref. [24]. Nevertheless, this region of the spectra is still under careful examination. In the following, we are focusing only on the RBM frequencies for which a small uniaxial strain has undetectable effects [24].

Figure 3 shows the Raman spectra and the diffraction patterns of the two tubes with the largest diameters of our data set, respectively, the (27, 4) and the (23, 21) SWNTs. The diameters of these semiconducting nanotubes are 2.287 and 2.984 nm (with $a_{C-C} = 0.142$ nm) and their chiral angles are 6.8° and 28.5° , respectively. The RBM are located at 119 cm^{-1} (FWHM = 11 cm^{-1}) and 95 cm^{-1} (FWHM = 13 cm^{-1}) for the (27, 4) and (23, 21) tubes, respectively [Figs. 3(a) and 3(b)].

A huge number of experiments and modelization efforts were made to relate the RBM frequency to the nanotube structure. A review and summary of various models and experiments is given in Ref. [2]. Our experimental approach provides the first accurate and independent determination of the lattice structure of the tubes, (n, m) indices, and then the diameters and chiral angles of all the tubes investigated, with their RBM frequencies. Figure 4 plots

the experimental relation between the RBM frequencies and the nanotube diameters obtained in this way. We want to point out that these results are covering an unprecedented diameter range (1.4–3 nm).

In Fig. 4, all the measured points agree with a line obeying the relation $\omega_{\text{RBM}} = A/d + B$, with $A = 204\text{ cm}^{-1}\text{ nm}$ and $B = 27\text{ cm}^{-1}$. We point out that this RBM vs diameter relation is measured on individual free-standing tubes, while, in previously established relations, the individual nanotubes were lying on a substrate [6] or encapsulated in surfactant [4,5,7]. Yet, we find a good agreement in the diameter range between 1.4 and 1.7 nm, where our diameter range overlaps with the previous works. This suggests that the previously established relationships cannot be extrapolated to the large diameter nanotubes that are present in our samples.

Our results allow one to discuss the structural (n, m) determination of Ref. [6] based only on resonant Raman scattering data obtained by using the 1.58 eV laser excitation. Indeed, we have measured the RBM frequencies of the (16, 7) and (15, 6) metallic tubes, and the RBM frequencies of these same tubes are given in Table I of Ref. [6]. A comparison between the two data sets shows complete agreement for (16, 7), since we found $\omega_{\text{RBM}} = 154\text{ cm}^{-1}$ ($E_{\text{laser}} = 1.57\text{ eV}$). Concerning (15, 6), the RBM is located at 166 cm^{-1} (165 cm^{-1} in Ref. [6]). It can be pointed out that our spectrum is recorded by using the 1.7 eV laser excitation and at 1.58 eV in Ref. [6]. On this point, our results seem supported by nonorthogonal

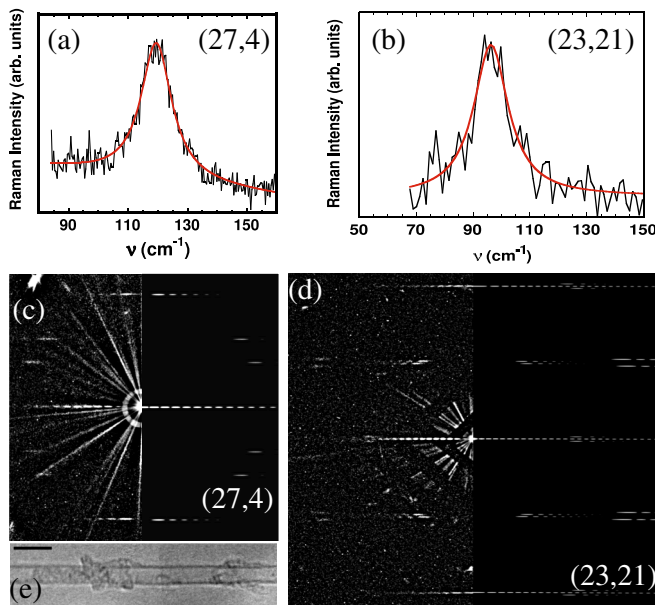


FIG. 3 (color online). (a) RBM of the (27, 4) SWNT ($E_{\text{Laser}} = 1.92\text{ eV}$) and (b) RBM of the (23, 21) nanotube ($E_{\text{Laser}} = 1.6\text{ eV}$). The electron diffraction patterns are shown in (c) and (d). In each pattern, the left half is the experimental image, while the right half is the simulated one for comparison. (e) High-resolution image of the (27, 4) SWNT. Scale bar is 5 nm.

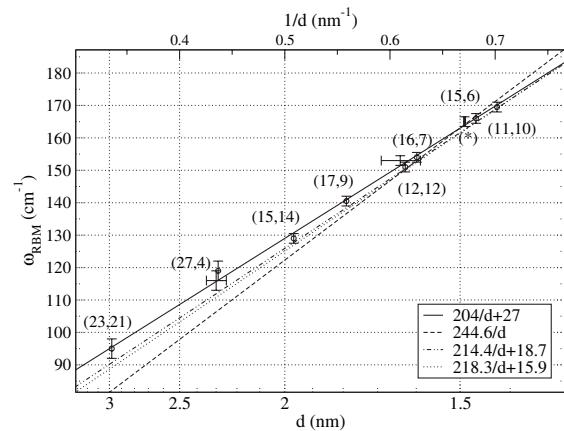


FIG. 4. RBM frequencies vs nanotube diameter d and inverse nanotube diameter $1/d$ for nanotubes identified by electron diffraction (see additional materials [21]). Data points marked with a circle are from unambiguously identified nanotubes, and the indices are given in the diagram. For the data points with a horizontal error bar, only a diameter estimate was possible. The data point marked with a star is from either a (16, 5) or a (18, 2), which have almost the same diameter (two tubes under the laser spot). Drawn as dashed lines are selected RBM vs diameter relationships from the literature [5–7] (the values from Ref. [6] are modified for a C-C bond length of 1.42 Å instead of 1.44 Å). The solid line is a linear fit to our data.

tight-binding calculations, which predict a ≈ 0.1 eV relative difference for the separation energies between Van Hove singularities of these two nanotubes [25]. Once more, an exact determination of the resonant energies would, however, require a full set of laser lines [4,5,7].

The present combined electron diffraction and Raman scattering experiments on the same freestanding SWNT is a direct measurement of the relation between the RBM frequency and the tube diameter without modelizations of the vibrational and electronic properties. For isolated tubes, the models predict a $\omega_{\text{RBM}} = A/d$ relation [2]. From the Raman experiments performed on surfactant wrapped individual SWNTs [4,5,7], a $\omega_{\text{RBM}} = A/d + B$ relation was found. The nonzero value of the B parameter is commonly attributed to the effect of the environment. Since most of the environmental influences are absent for the freestanding SWNTs investigated, this assumption seems questionable in our case. Our results suggest, rather, that the dependence of RBM frequency with the inverse of the diameter might be slightly nonlinear. Further, the precise agreement between RBM frequencies for identified tubes in surfactant or on a substrate with our data on freestanding tubes shows that the influence of the environment is rather small. It was shown by first principles calculations [26,27] that the RBM vs d relation is nonlinear for tubes with very small diameters. However, the predicted deviations from a linear behavior are significant only for nanotubes smaller than 1 nm, which is much smaller than the diameters investigated here. To elucidate definitely these points, investigations on well characterized (n, m) freestanding nanotubes of small diameter are in progress. The expected results will allow a direct comparison with more of the experimental results obtained from surfactant wrapped individual SWNTs [4,5,7] and *ab initio* calculations [22].

In conclusion, we have obtained the Raman spectra of (n, m) nanotubes well characterized by electron diffraction and high-resolution TEM imaging. We have directly measured the radial breathing mode frequency for a wide range of diameters. Both the micro-Raman spectroscopy and the electron microscopic investigation are done on a freely suspended object without an influence from a substrate, surfactant, or contacts. Our measurements, carried out on a wide range of diameters from 1.4 nm up to 3 nm, confirm the previously established more or less model dependent laws in the range 1.4–1.7 nm, in spite of the different environment. This raises questions on the interpretation of the environmental constant. The unprecedented study of large diameter tubes shows that the RBM frequency is not simply inversely proportional to the nanotube diameter.

The measurement of vibrational modes for a precisely known structure can provide a direct test for molecular dynamics simulations. Further, we expect that the procedure shown here can be adopted to various nano-objects or

macromolecules to combine electron microscopic structural analysis with Raman spectroscopy and potentially other investigations on the same object.

This work has been done in the framework of the GDRE No. 2756 “Sciences and applications of the nanotubes—NANO-E.” The authors acknowledge financial support by the EU projects CARDECOM and CANAPE and the BMBF project INKONAMI. We thank xlith.com for lithography services. We thank P. Poncharal, A. Zahab, C. Koch, K. Hahn, M. Kelsch, F. Phillipp, and M. Rühle for support and helpful discussions.

*Electronic address: email@jannikmeyer.de

†Electronic address: paillet@lcvn.univ-montp2.fr

- [1] R. Saito, G. Dresselhaus, and M. S. Dresselhaus, *Physical Properties of Carbon Nanotubes* (Imperial College Press, London, 1998).
- [2] S. Reich, C. Thomsen, and J. Maultzsch, *Carbon Nanotubes. Basic Concepts and Physical Properties* (Wiley-VCH, Weinheim, Germany, 2004).
- [3] M. Dresselhaus *et al.*, Phys. Rep. **409**, 47 (2005).
- [4] C. Fantini *et al.*, Phys. Rev. Lett. **93**, 147406 (2004).
- [5] H. Telg *et al.*, Phys. Rev. Lett. **93**, 177401 (2004).
- [6] A. Jorio *et al.*, Phys. Rev. Lett. **86**, 1118 (2001).
- [7] A. Jorio *et al.*, Phys. Rev. B **71**, 075401 (2005).
- [8] J. Kürti, G. Kresse, and H. Kuzmany, Phys. Rev. B **58**, R8869 (1998).
- [9] D. Sánchez-Portal *et al.*, Phys. Rev. B **59**, 12 678 (1999).
- [10] M. Gao *et al.*, Appl. Phys. Lett. **82**, 2703 (2003).
- [11] L. C. Qin, T. Ichihashi, and S. Iijima, Ultramicroscopy **67**, 181 (1997).
- [12] S. Amelinckx, A. Lucas, and P. Lambin, Rep. Prog. Phys. **62**, 1471 (1999).
- [13] A. A. Lucas, V. Bruyninckx, and P. Lambin, Europhys. Lett. **35**, 355 (1996).
- [14] J. M. Cowley *et al.*, Chem. Phys. Lett. **265**, 379 (1997).
- [15] J.-F. Colomer *et al.*, Phys. Rev. B **70**, 075408 (2004).
- [16] J. C. Meyer *et al.*, cond-mat/0506356 [Ultramicroscopy (to be published)].
- [17] J. C. Meyer *et al.*, Appl. Phys. Lett. **85**, 2911 (2004).
- [18] M. Paillet *et al.*, J. Phys. Chem. B **108**, 17 112 (2004).
- [19] Y. Zhang and H. Dai, Appl. Phys. Lett. **77**, 3015 (2000).
- [20] Y. Zhang *et al.*, Chem. Phys. Lett. **331**, 35 (2000).
- [21] See EPAPS Document No. E-PRLTAO-95-082547 for a table of the structural indices. This document can be reached via a direct link in the online article’s HTML reference section or via the EPAPS homepage (<http://www.aip.org/pubservs/epaps.html>).
- [22] O. Dubay, G. Kresse, and H. Kuzmany, Phys. Rev. Lett. **88**, 235506 (2002).
- [23] A. Jorio *et al.*, Phys. Rev. Lett. **90**, 107403 (2003).
- [24] S. B. Cronin *et al.*, Phys. Rev. Lett. **93**, 167401 (2004).
- [25] V. N. Popov and L. Henrard, Phys. Rev. B **70**, 115407 (2004).
- [26] J. Kürti *et al.*, New J. Phys. **5**, 125 (2003).
- [27] J. Kürti *et al.*, Carbon **42**, 971 (2004).